Proceedings of the Combustion Institute 40 (2024) 105687

Contents lists available at ScienceDirect

Proceedings of the Combustion Institute

journal homepage: www.elsevier.com/locate/proci

Area increase and stretch factor in lean hydrogen-air turbulent flames

H.C. Lee [a,b], B. Wu [a], P. Dai [a,*], M. Wan [a,b,c], Andrei N. Lipatnikov [d]

[a] Guangdong Provincial Key Laboratory of Turbulence Research and Applications, Department of Mechanics and Aerospace Engineering, Southern University of Science and Technology, Shenzhen 518055, PR China
[b] Guangdong-Hong Kong-Macao Joint Laboratory for Data-Driven Fluid Mechanics and Engineering Applications, Southern University of Science and Technology, Shenzhen 518055, PR China
[c] Jiaxing Research Institute, Southern University of Science and Technology, Jiaxing, Zhejiang 314031, PR China
[d] Department of Mechanics and Maritime Sciences, Chalmers University of Technology, Gothenburg SE-412 96, Sweden

ARTICLE INFO

Keywords:
Premixed turbulent combustion
Flame speed
Flame surface area
Stretch factor
Differential diffusion
Lewis number
Thermodiffusive instability

ABSTRACT

Analyzed in this paper are three-dimensional Direct Numerical Simulation (DNS) data obtained earlier by the present authors from (i) 16 statistically planar and one-dimensional, lean complex-chemistry hydrogen-air turbulent flames propagating in forced turbulence in a box and (ii) nine counterpart equidiffusive flames. The simulation conditions cover a wide range of non-dimensional turbulent combustion characteristics. Specifically, root-mean-square turbulent velocity is varied from 0.3 to 55 laminar flame speeds, integral length scale of turbulence is varied from 0.5 to 2.6 laminar flame thicknesses, Damköhler and Karlovitz number are varied from 0.01 to 5.2 and from 0.7 to 1300, respectively. Three equivalence ratios, 0.7, 0.5, and 0.35, are addressed. Results of complementary two- and three-dimensional simulations of thermodiffusively unstable laminar flames are also reported. They show that neutral wavelength of laminar flame instabilities (both hydrodynamic and thermodiffusive ones are enabled in the simulations) is smaller (larger) than computational domain wide in ten (three, respectively) cases characterized by a low Lewis number. Accordingly, in three of these cases, the instabilities are suppressed. The focus of the study is placed (i) on contributions of flame surface area increase and stretch factor to turbulent burning velocity and (ii) on the influence of differential diffusion effects on these contributions. The computed results show that the flame surface area (i) is substantially increased by both turbulent rms velocity and length scale, (ii) is mainly controlled by turbulence, but (iii) is weakly affected by an increase in Lewis number. On the contrary, the stretch factor (i) is much larger than unity in low Lewis number flames, (ii) is significantly increased with decreasing equivalence ratio, and (iii) is weakly increased by rms turbulent velocity, but (iv) a notable influence of turbulence length scale on the stretch factor is not observed.

1. Introduction

Various models [1–4] of the influence of turbulence on burning rate separate large-scale and small-scale effects, which are often associated with an increase in flame surface wrinkled by larger eddies and variations in the local flame structure stretched by smaller eddies, respectively. Such a paradigm goes back to the pioneering work by Damköhler [5] who highlighted an increase Σ in flame surface area but did not consider variations in the local flame structure. Later, such variations were proposed [6,7] to be modeled using a stretch factor I, which quantified difference in a mean local consumption velocity $\overline{u}_c$ in a turbulent flow and the speed S_L^0 of the unperturbed (stationary, planar, and one-dimensional) laminar flame. Accordingly, turbulent burning velocity U_T is often estimated [1–4] to be a product of S_L^0, Σ, and I, i.e.,

$$U_T = S_L^0 \Sigma I. \quad (1)$$

If molecular diffusivities of fuel and oxygen are close to one another and Lewis number $Le = a/D \geq 1$, low values of $I < 1$ are commonly expected in sufficiently intense turbulence [6,7] due to reduction in $\overline{u}_c$ by turbulent stretching and local combustion quenching. Here, a and D designate molecular heat diffusivity of a mixture and molecular diffusivity of deficient reactant in that mixture. Nevertheless, recent Direct Numerical Simulation (DNS) studies [8–12] have indicated that the simple Eq. (1) can well perform even if the factor I is set equal to unity in highly turbulent flames characterized by Karlovitz numbers $Ka \approx \tau_F/\tau_K$ larger than unity. Here, the time scale $\tau_F = \delta_L/S_L^0$ characterizes the

* Corresponding author.
E-mail address: daip@sustech.edu.cn (P. Dai).

https://doi.org/10.1016/j.proci.2024.105687
Received 4 December 2023; Accepted 21 July 2024
Available online 19 August 2024

Table 1
Major characteristics of simulated flames.

Gr.	Case	Φ	S_L^0, m/s	δ_L^T, mm	*Le*	$\frac{u'}{S_L^0}$	$\frac{L}{\delta_L^T}$	*Da*	*Ka*	Re_λ	$\frac{\Delta x}{\eta}$	*N*	*M*	Λ, mm	
I	$\mathscr{T}_S\phi_{0.5}$A	0.5	0.58	0.41	0.39	0.34	0.61	1.8	1.0	3.6	0.22	64	16	1.32	U
	$\mathscr{T}_S\phi_{0.5}$B	0.5	0.58	0.41	0.39	1.0	0.61	0.6	4.2	10	0.25	128	16	1.32	U
	$\mathscr{T}_S\phi_{0.5}$B1	0.5	0.78	0.29	1.0	0.74	0.86	1.2	4.2	9.4	0.40	128	16		S
II	$\mathscr{T}_M\phi_{0.5}$A	0.5	0.58	0.41	0.39	1.0	1.1	1.1	3.5	14	0.24	128	16	2.4	U
	$\mathscr{T}_M\phi_{0.5}$A1	0.5	0.78	0.29	1.0	0.74	1.6	2.1	3.3	14	0.40	128	16		S
	$\mathscr{T}_M\phi_{0.5}$B	0.5	0.58	0.41	0.39	2.2	1.1	0.53	9.9	21	1.08	64	18	2.4	U
	$\mathscr{T}_M\phi_{0.5}$B1	0.5	0.78	0.29	1.0	1.6	1.6	1.0	5.4	19	1.08	64	18		S
	$\mathscr{T}_M\phi_{0.5}$C	0.5	0.58	0.41	0.39	4.0	1.1	0.29	26.0	26	1.13	96	18	2.4	U
	$\mathscr{T}_M\phi_{0.5}$C1	0.5	0.78	0.29	1.0	3.0	1.6	0.54	13.9	26	1.13	96	18		S
	$\mathscr{T}_M\phi_{0.5}$D	0.5	0.58	0.41	0.39	11.2	1.1	0.10	121.	44	1.85	128	16	2.4	U
	$\mathscr{T}_M\phi_{0.5}$D1	0.5	0.78	0.29	1.0	8.3	1.6	0.19	66.6	43	1.85	128	16		S
III	$\mathscr{T}_L\phi_{0.5}$A	0.5	0.58	0.41	0.39	0.25	2.6	10.4	1.2	4.9	0.10	256	12	5.6	U
	$\mathscr{T}_L\phi_{0.5}$B	0.5	0.58	0.41	0.39	0.5	2.6	5.2	1.5	10	0.17	256	12	5.6	U
	$\mathscr{T}_L\phi_{0.5}$C	0.5	0.58	0.41	0.39	1.0	2.6	2.6	2.1	22	0.29	256	12	5.6	U
	$\mathscr{T}_L\phi_{0.5}$D	0.5	0.58	0.41	0.39	1.5	2.6	1.8	3.9	27	0.39	256	12	5.6	U
	$\mathscr{T}_L\phi_{0.5}$E	0.5	0.58	0.41	0.39	2.0	2.6	1.3	6.4	28	0.51	256	12	5.6	U
	$\mathscr{T}_L\phi_{0.43}$E1	0.43	0.58	0.31	1.0	2.0	3.4	1.5	4.9	28	0.51	256	12		S
IV	$\mathscr{T}_s\phi_{0.35}$A	0.35	0.12	0.92	0.36	11.2	0.5	0.04	125.	20	1.13	64	16	2.4	S
	$\mathscr{T}_s\phi_{0.35}$A1	0.35	0.30	0.43	1.0	4.5	1.1	0.24	24.3	20	1.13	64	16		S
	$\mathscr{T}_s\phi_{0.35}$B	0.35	0.12	0.92	0.36	54.1	0.5	0.01	1315.	44	1.85	128	16	2.4	S
	$\mathscr{T}_s\phi_{0.35}$B1	0.35	0.30	0.43	1.0	21.6	1.1	0.05	268.	41	1.85	128	16		S
V	$\mathscr{L}\phi_{0.5}$A(S)	0.5	0.58	0.41	0.39	1.0	0.58	0.6	4.1	11	0.24	128	16	1.26	S
	$\mathscr{L}\phi_{0.5}$A(U)	0.5	0.58	0.41	0.39	1.0	0.61	0.6	4.2	10	0.25	128	16	1.32	U
	$\mathscr{L}\phi_{0.5}$A1	0.5	0.78	0.29	1.0	0.74	0.86	1.2	4.2	9.4	0.40	128	16		S
	$\mathscr{L}\phi_{0.5}$B	0.5	0.58	0.41	0.39	1.0	1.1	1.1	3.5	14	0.24	128	16	2.4	U
	$\mathscr{L}\phi_{0.5}$B1	0.5	0.78	0.29	1.0	0.74	1.6	2.1	3.3	14	0.40	128	16		S
	$\mathscr{L}\phi_{0.5}$C	0.5	0.58	0.41	0.39	1.0	2.6	2.6	2.1	22	0.29	256	12	5.6	U
VI	$\mathscr{L}\phi_{0.35}$A	0.35	0.12	0.92	0.36	11.2	0.5	0.04	125.	20	1.13	64	16	2.4	S
	$\mathscr{L}\phi_{0.35}$A1	0.35	0.30	0.43	1.0	4.5	1.1	0.24	24.3	20	1.13	64	16		S
	$\mathscr{L}\phi_{0.35}$B	0.35	0.12	0.92	0.36	11.2	1.2	0.10	85.7	29	1.07	128	16	5.6	U
	$\mathscr{L}\phi_{0.35}$B1	0.35	0.30	0.43	1.0	4.5	2.5	0.56	85.7	28	1.07	128	16		S
	$\phi_{0.7}$	0.70	1.42	0.34	0.41	4.6	1.3	0.29	41	51	1.48	160	16	2.4	

unperturbed laminar flame of thickness δ_L and the Kolmogorov time scale τ_K characterizes small-scale turbulence. Accordingly, numerous data on U_T/S_L^0, reviewed elsewhere [4,13], are also directly relevant to the area increase Σ under conditions associated with $I \cong 1$.

However, a simplification of $I = 1$ does not work in turbulent flames characterized by a low *Le*, e.g., in very lean H_2-air mixtures. In such flames, abnormally high ratios of U_T/S_L^0 were documented in numerous experimental studies reviewed elsewhere [14–16]. This effect is commonly attributed to local variations in temperature and mixture composition due to imbalance of molecular fluxes of heat and chemical energy from and to, respectively, inherently laminar reaction zones stretched by turbulent eddies [14–18]. To allow for such effects, the stretch factor should be significantly larger than unity.

While large values of $I > 1$ were indeed reported in recent DNS studies of lean H_2-air turbulent flames [19–22], investigations of (i) the influence of *Le* on Σ or/and (ii) the behavior of the stretch factor *I* in premixed turbulent flames characterized by a low *Le* have yet been limited. Specifically, as far as complex-chemistry DNSs of turbulent burning of lean H_2-containing mixtures are concerned, Berger et al. [19, Fig. 7] reported $I \approx 5$ and weak differences in Σ obtained from low *Le* and equidiffusive (i.e., molecular diffusivities of all species are changed to *a*, with all other things being equal) flames, but that study was restricted to a single jet flame. DNS data by Rieth et al. [20, Fig. 9c] also imply weak influence of *Le* on Σ in a single case, but the stretch factor *I* was not addressed in the cited paper. Lee et al. [23] reported weak differences in Σ obtained from low *Le* and equidiffusive flames in four cases, but the stretch factor *I* was beyond the focus of that study. Rieth et al. [24, Fig. 18] documented *I* as large as seven but discussed neither its dependence on the equivalence ratio Φ and turbulence characteristics nor the influence of *Le* on Σ. Finally, Howarth et al. [21] simulated 33 turbulent flames and reported an increase in $\overline{u}_c$ by *Ka*. However, the focus of the study was placed on variations in pressure and temperature. Accordingly, there were only four cases "A" characterized by different rms velocities u', the same turbulence length scale *L*, and the same Φ, but there were no cases characterized by different Φ or *L* and the same values of the two other quantities, i.e., u' and *L* or u' and Φ, respectively. Moreover, the influence of *Le* on Σ was beyond the scope of the cited work.

To bridge the knowledge gaps outlined above, the present work aims at (i) comparing contributions of Σ and *I* to an increase in U_T/S_L^0 in low Lewis number flames and (ii) systematically exploring dependencies of the area increase Σ and the stretch factor *I* on turbulence and mixture characteristics by analyzing DNS data obtained from 16 lean hydrogen-air turbulent premixed flames and nine counterpart equidiffusive flames in a wide range of conditions ($u'/S_L^0 = 0.34 \div 54$, $L/\delta_L = 0.43 \div 2.6$; $\Phi = 0.35$ 0.5, and 0.7). As those simulations were discussed in detail in our earlier papers [11,23,25–30], the DNS attributes are briefly reported in Sect. 2. Results are discussed in Sect. 3, followed by conclusions.

2. DNS attributes and diagnostic methods

DNS data analyzed in the following were obtained from statistically planar and one-dimensional, complex-chemistry, lean H_2-air flames propagating against incoming reactant flow in a box $\Lambda \times M\Lambda \times \Lambda$ along *y*-direction. For this purpose, unsteady, three-dimensional continuity, Navier-Stokes, energy, and species transport equations written in the low-Mach-number formulation were numerically solved using software DINO [31], a chemical mechanism by Kéromnès et al. [32], and mixture-averaged molecular transport model [33]. Numerical meshes consisted of $N \times MN \times N$ cells. The width Λ and the numbers *M* and *N*

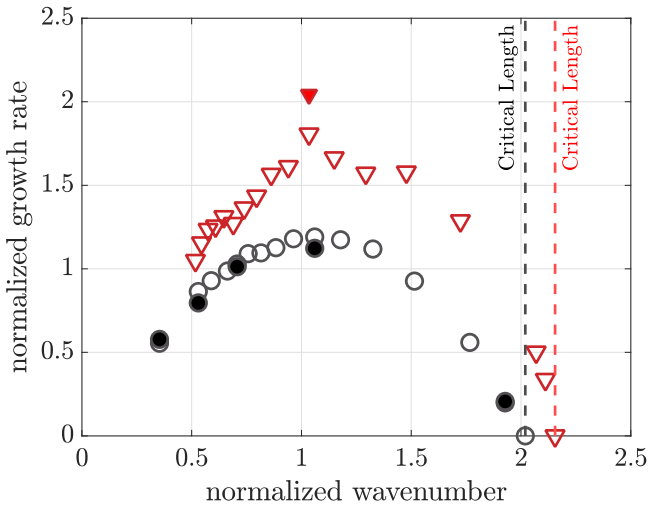

Fig. 1. Normalized instability growth rate $\tau_F\omega$ vs. normalized wavenumber $\delta_L^T k$. Open and filled symbols show results obtained in two- and three-dimensional simulations, respectively. Black circles and red triangles show results obtained at $\Phi = 0.5$ and 0.35, respectively.

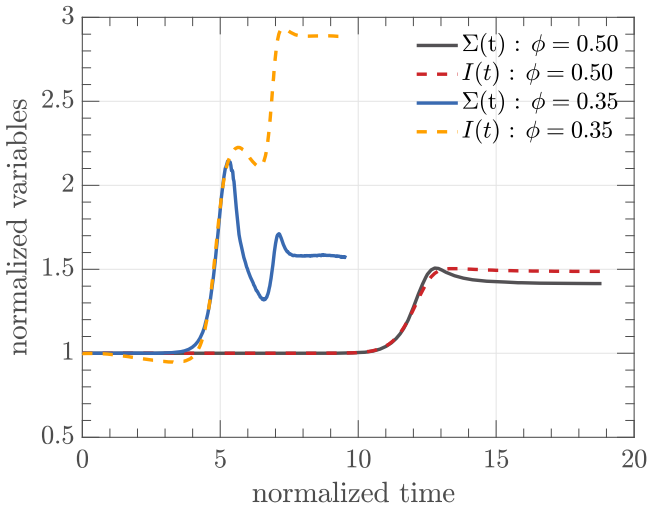

Fig. 2. Evolution of flame-surface-area increase $\Sigma(t)$ (black and blue solid lines) and stretch factor $I(t)$ (red and yellow dashed lines) in unstable laminar flames characterized by $\Phi = 0.5$, $\lambda = \Lambda = 2.4$mm (black and red lines) or $\Phi = 0.35$, $\lambda = \Lambda = 5.6$mm (blue and yellow lines).

are specified in Table 1. Along the streamwise direction, inflow and outflow boundary conditions were set. Other boundary conditions were periodic.

Turbulence was generated adopting linear forcing method [34–36], specifically, its variable-density modification introduced by Bobbit et al. [37,38]. This method yields "the correct scaling of the energy spectrum and capture accurately the energy cascade at the large scales" [37, p. 8 and Fig. 3]. Moreover, the method offers the opportunity to maintain roughly the same target value of transverse-averaged turbulent kinetic energy both upstream and within entire mean flame brush, as reported elsewhere [26]. Combustion simulations were started by embedding a pre-computed planar laminar flame in the center of the computational domain, i.e., at $y = M\Lambda/2$, at $t = 0$.

Major characteristics of the studied flames are reported in Table 1, where u' and $L = u'^3/\varepsilon_0$ are target values of turbulent rms velocity and integral length scale, respectively; $\varepsilon_0 = 2\nu\langle S_{ij}S_{ij}\rangle$ is dissipation rate averaged over forced turbulence volume before embedding a flame; ν is kinematic viscosity of fresh gas; $S_{ij} = \left(\partial u_i/\partial x_j + \partial u_j/\partial x_i\right)/2$ is the rate-of-strain tensor; and the summation convention applies to repeated indexes. The linear forcing method yields $L = 0.19\Lambda$ [26,37,38]. The unperturbed laminar flame speed S_L^0, thickness $\delta_L^T = (T_b - T_u)/\max|\nabla T|$, and time scale $\tau_F = \delta_L^T/S_L^0$ are computed using the same chemical mechanism [32] and software Cantera [33]. Here, T is the temperature and subscript u or b refers to unburned or burned gas, respectively. The Reynolds number $Re_\lambda = u'\lambda/\nu$, Damköhler number $Da = \tau_t/\tau_F$, and Karlovitz number $Ka = \tau_F/\tau_K$ are evaluated using Taylor microscale $\lambda = (10\nu_u u'/\varepsilon_{le})^{1/2}$, integral time scale $\tau_t = L/u'$, and Kolmogorov time scale $\tau_K = (\nu_u/\varepsilon_{le})^{1/2}$. Here, the dissipation rate ε_{le} is averaged over flame-brush leading zone where transverse-averaged combustion progress variable $0.01 < \overline{c}_F(y,t) < 0.05$. It is defined using fuel mass fraction Y_F, i.e., $c_F = 1 - Y_F/Y_{F,u}$. Finally, Δx is grid spacing, $\eta_K = \left(\nu^3/\varepsilon_{le}\right)^{1/4}$ is Kolmogorov length scale, $Le = a_u/D_{H_2,u}$, letters U (unstable) and S (stable) in the last column indicate whether thermodiffusive instability of laminar flames can affect the turbulent flames. The instability cannot appear in equidiffusive cases or if the domain width Λ is smaller than the instability neutral wavelength Λ_n, see Fig. 1 discussed in Section 3. If $\Lambda > \Lambda_n$, the instability can appear, and such cases are marked with U. The bottom right cell is empty in the moderately lean case F7, as it is not known whether this mixture is thermodiffusively unstable.

To investigate the influence of differential diffusion on combustion characteristics, certain low Le flames are accompanied with equidiffusive flames, which are marked with the number 1 in the end of the case names. Furthermore, to explore effects due to variations in (i) u'/S_L^0, (ii) L/δ_L^T, or (iii) Φ by retaining two other parameters unchanged, the DNS conditions are divided in six groups I-VI, based on characteristics of the low Le flames. These six groups are separated with horizontal dashed lines in Table 1.

Specifically, in each group, the equivalence ratio is kept constant and equal either to 0.5 or to 0.35 (a single flame $\phi_{0.7}$ characterized by $\Phi = 0.7$ does not belong to any group, see the bottom row in Table 1). Accordingly, symbol $\phi_{0.5}$ or $\phi_{0.35}$ in the middle of a case name refers to $\Phi = 0.5$ or 0.35, respectively. All low Le flames in each of the first four groups are characterized by the same L/δ_L^T, with the subscript (S, M, or L) after the first letter $\mathscr{D}$ ("domain") in the case name referring to L/δ_L^T (small, medium, or large, respectively). Within each of these four groups, u'/S_L^0 is increased from case A to case B, D, or E, see the last capital letters in the case names, used also in Refs. [11,23,25–30]. Similarly, all low Le flames in the fifth and sixth groups are characterized by the same u'/S_L^0 but different L/δ_L^T, as indicated with the first letter $\mathscr{L}$ in the case names. Within each of these two groups, L/δ_L^T is increased from case A to case B or C.

For each of the six groups to cover a wider range of variations in u'/S_L^0 or L/δ_L^T, four low Le flames and their equiduffusive counterparts are included with different names in two groups each. These are cases (i) $\mathscr{D}_S\phi_{0.5}$B and $\mathscr{L}\phi_{0.5}$A(U) in groups I and V, (ii) $\mathscr{D}_M\phi_{0.5}$A and $\mathscr{L}\phi_{0.5}$B in groups II and V, (iii) $\mathscr{D}_L\phi_{0.5}$C and $\mathscr{L}\phi_{0.5}$C in groups III and V, (iv) $\mathscr{D}_S\phi_{0.35}$A and $\mathscr{L}\phi_{0.35}$A in groups IV and VI.

Flames $\mathscr{D}_M\phi_{0.5}$B, $\mathscr{D}_M\phi_{0.5}$C, $\mathscr{D}_M\phi_{0.5}$D, $\mathscr{D}_S\phi_{0.35}$B, $\mathscr{D}_S\phi_{0.35}$A/$\mathscr{L}\phi_{0.35}$A, and $\mathscr{L}\phi_{0.35}$B (as well as their equidiffusive counterparts) were discussed in earlier papers [11,23,25–29], where these flames are labeled A, B, C, D, E, and F, respectively (or A1-F1, respectively). Flame $\phi_{0.7}$ is discussed in Ref. [29], where this case is simply labeled G. Moreover, flames $\mathscr{D}_S\phi_{0.5}$A,$\mathscr{D}_S\phi_{0.5}$B/$\mathscr{L}\phi_{0.5}$A(U), $\mathscr{L}\phi_{0.5}$A, and $\mathscr{D}_M\phi_{0.5}$A/$\mathscr{L}\phi_{0.5}$B or their equidiffusive counterparts were discussed in another paper [30], where these flames are labeled LT/U, T/U, T/S, and T/UM, respectively, or T/U1 and T/UM1, respectively. Five new cases $\mathscr{D}_L\phi_{0.5}$A - $\mathscr{D}_L\phi_{0.5}$E in group III were designed to assess the following criterion $Ka < Ka_{cr} = \sqrt{15}\tau_F\max\{\omega(k)\}$ [39] of importance of thermodiffusive instability of laminar flames in turbulent flows. From this perspective, these DNS data will be explored in a future publication,

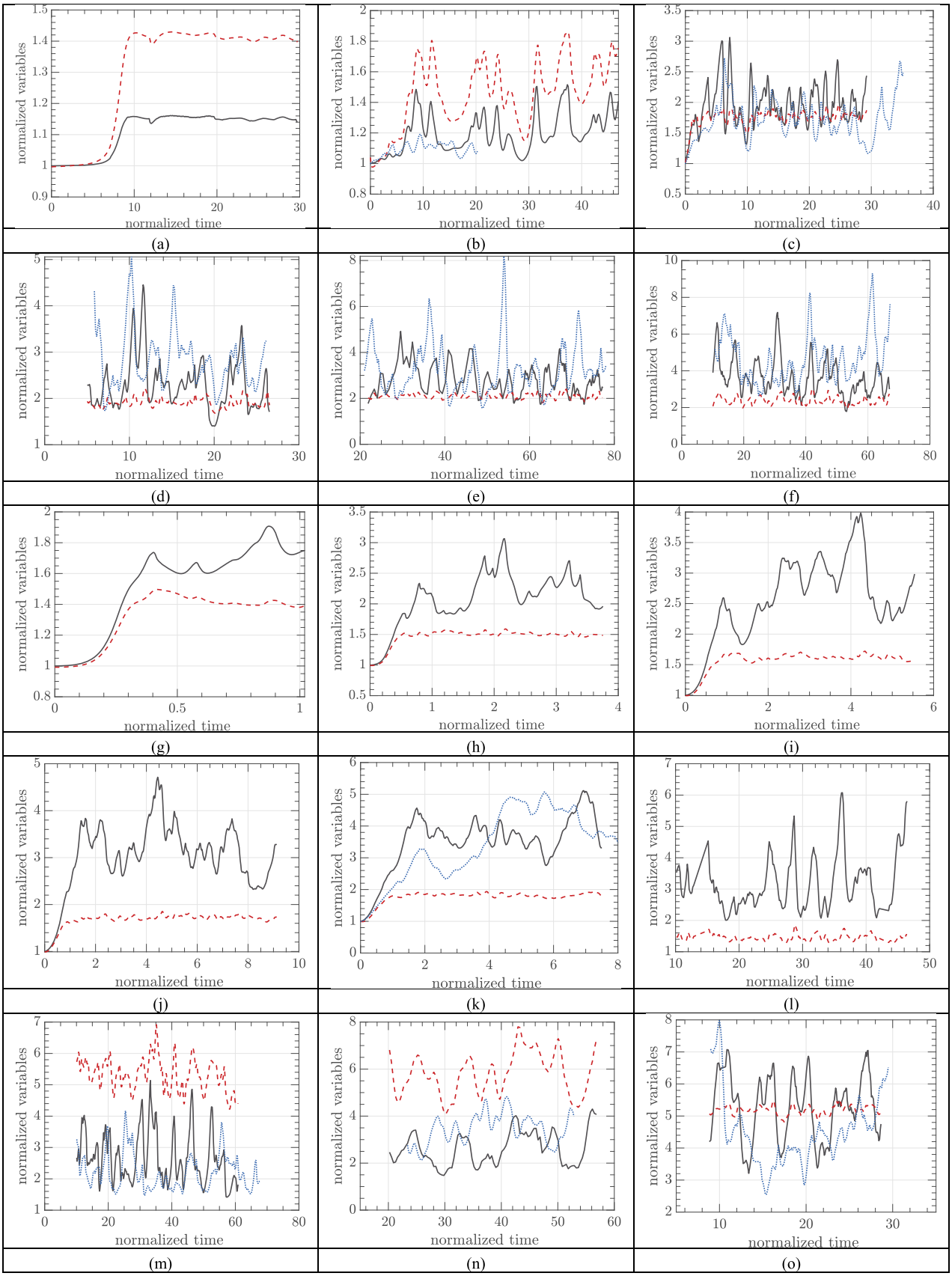

Fig. 3. Area-factor Σ (black solid lines) and stretch factor I (red dashed lines). Area factors obtained from equidiffusive flames are plotted in blue dotted lines. (a) $\mathscr{S}_S\phi_{0.5}$A, (b) $\mathscr{S}_S\phi_{0.5}$B and $\mathscr{S}_S\phi_{0.5}$B1, (c) $\mathscr{S}_M\phi_{0.5}$A and $\mathscr{S}_M\phi_{0.5}$A1, (d) $\mathscr{S}_M\phi_{0.5}$B and $\mathscr{S}_M\phi_{0.5}$B1, (e) $\mathscr{S}_M\phi_{0.5}$C and $\mathscr{S}_M\phi_{0.5}$C1, (f) $\mathscr{S}_M\phi_{0.5}$D and $\mathscr{S}_M\phi_{0.5}$D1, (g) $\mathscr{S}_L\phi_{0.5}$A, (h) $\mathscr{S}_L\phi_{0.5}$B, (i) $\mathscr{S}_L\phi_{0.5}$C, (j) $\mathscr{S}_L\phi_{0.5}$D, (k) $\mathscr{S}_L\phi_{0.5}$E and $\mathscr{S}_L\phi_{0.43}$E1, (l) $\phi_{0.7}$, (m) $\mathscr{S}_S\phi_{0.35}$A and $\mathscr{S}_S\phi_{0.35}$A1, (n) $\mathscr{S}_S\phi_{0.35}$B and $\mathscr{S}_S\phi_{0.35}$B1, and (o) $\mathscr{L}\phi_{0.35}$B.

Table 2
Time-averaged area-factor, stretch factor, and burning velocity in groups I-IV where u'/S_L^0 is varied by retaining L/δ_L^T.

Group	I, $\Phi = 0.5$			II, $\Phi = 0.5$							
Case	$\mathscr{D}_S\phi_{0.5}$A	$\mathscr{D}_S\phi_{0.5}$B	$\mathscr{D}_S\phi_{0.5}$B1	$\mathscr{D}_M\phi_{0.5}$A	$\mathscr{D}_M\phi_{0.5}$A1	$\mathscr{D}_M\phi_{0.5}$B	$\mathscr{D}_M\phi_{0.5}$B1	$\mathscr{D}_M\phi_{0.5}$C	$\mathscr{D}_M\phi_{0.5}$C1	$\mathscr{D}_M\phi_{0.5}$D	$\mathscr{D}_M\phi_{0.5}$D1
$\overline{\Sigma(t)}$	1.2	1.2	1.1	1.8	1.7	2.1	2.8	2.5	3.3	3.3	4.3
$\overline{I(t)}$	1.4	1.5	1.0	1.8	1.0	1.9	1.0	2.1	1.0	2.4	1.0
$\overline{U_T(t)}$	1.7	1.8	1.1	3.2	1.7	4.0	2.8	5.4	3.3	7.9	4.3

Group	III, $\Phi = 0.5$						IV, $\Phi = 0.35$			
Case	$\mathscr{D}_L\phi_{0.5}$A	$\mathscr{D}_L\phi_{0.5}$B	$\mathscr{D}_L\phi_{0.5}$C	$\mathscr{D}_L\phi_{0.5}$D	$\mathscr{D}_L\phi_{0.5}$E	$\mathscr{D}_L\phi_{0.43}$E1	$\mathscr{D}_S\phi_{0.35}$A	$\mathscr{D}_S\phi_{0.35}$A1	$\mathscr{D}_S\phi_{0.35}$B	$\mathscr{D}_S\phi_{0.35}$B1
$\overline{\Sigma(t)}$	1.7	2.1	2.5	3.2	3.8	3.9	2.2	2.2	2.6	3.6
$\overline{I(t)}$	1.4	1.5	1.6	1.7	1.8	1.0	5.3	1.0	5.8	1.0
$\overline{U_T(t)}$	2.3	3.2	4.0	5.4	6.8	3.9	12.1	2.2	15.1	3.6

Table 3
Time-averaged area-factor, stretch factor, and burning velocity in groups V and VI where L/δ_L^T is varied by retaining u'/S_L^0.

Group	V, $\Phi = 0.5$						VI, $\Phi = 0.35$			
case	$\mathscr{L}\phi_{0.5}$A(S)	$\mathscr{L}\phi_{0.5}$A(U)	$\mathscr{L}\phi_{0.5}$A1	$\mathscr{L}\phi_{0.5}$B	$\mathscr{L}\phi_{0.5}$B1	$\mathscr{L}\phi_{0.5}$C	$\mathscr{L}\phi_{0.35}$A	$\mathscr{L}\phi_{0.35}$A1	$\mathscr{L}\phi_{0.35}$B	$\mathscr{L}\phi_{0.35}$B1
$\overline{\Sigma(t)}$	1.2	1.2	1.1	1.8	1.7	2.5	2.3	2.2	4.4	4.3
$\overline{I(t)}$	1.5	1.5	1.0	1.8	1.0	1.6	5.3	1.0	5.2	1.0
$\overline{U_T(t)}$	1.8	1.8	1.1	3.2	1.7	4.0	12.1	2.2	23.9	4.3

whereas the present study is solely restricted to evaluating $U_T(t)$, $\Sigma(t)$ and $I(t)$.

When analyzing the DNS data [11,23,25–30], turbulent burning velocity is calculated by spatially integrating fuel consumption rate $\dot{\omega}_F(\mathbf{x},t)$, i.e.,

$$U_T(t) = -\frac{W_F}{\rho_u Y_{F,u} \Lambda^2} \int\int\int \dot{\omega}_F(\mathbf{x},t) d\mathbf{x}. \quad (2)$$

Here, W_F is fuel molecular weight, ρ is the density. The area-factor $\Sigma(t)$ is evaluated by measuring the instantaneous area of a surface of $c_F(\mathbf{x},t) = 0.5$. As discussed elsewhere [11, Fig. 1], this and other methods tested therein yield similar results. Finally, the stretch factor $I(t)$ is obtained using Eq. (1).

3. Results and discussion

3.1. Unstable laminar flames

To compare turbulent and unstable laminar flames, two- and three-dimensional simulations of the latter flames were also performed using the same software [31], the same chemical mechanism [32], and the same transport model [33], as discussed in detail in the case of $\Phi = 0.5$ elsewhere [30]. Dispersion relations $\omega(k)$ obtained by setting perturbation wavelength k equal to $2\pi/\Lambda$ and varying the width Λ are shown in Fig. 1. Here, ω is the instability (both thermodiffusive and hydrodynamical ones) growth rate found using a scaling of $\ln[U_L(t)/S_L - 1] \propto 2\omega t$, which results from the flame instability theory [40]. Similar dispersion curves were also computed by other groups [41, 42], while the normalized growth rates reported by us earlier [30, Fig. 2; 43, Fig. 3b] were evaluated using another fit, i.e., $U_L(t)/S_L \propto \exp(\omega t)$, and, hence, were underestimated by a factor of about two. The data plotted in Fig. 1 show that $Ka_{cr} = 4.3$ at $\Phi = 0.5$ and $Ka_{cr} = 7.7$ at $\Phi = 0.35$.

The normalized growth rates $\tau_F\omega$ obtained in two- and three-dimensional simulations are close to one another (cf. open and filled symbols). The neutral wavenumbers k_n such that $\omega(k \geq k_n) \leq 0$ are also almost the same in both cases. It is worth stressing that $\Lambda_n = 2\pi/k_n = 2.68$ mm is larger than the width $\Lambda = 2.4$mm of the domain used in the previous DNSs [23,28,29] of leaner ($\Phi = 0.35$) flames $\mathscr{D}_S\phi_{0.35}$B and $\mathscr{D}_S\phi_{0.35}$A/$\mathscr{L}\phi_{0.35}$A. Hence, laminar flame instabilities were not enabled in these two cases, as indicated using letter S in the last column in Table 1. Besides, $\Lambda_n = 1.3$mm is larger than the width Λ in flame $\mathscr{L}\phi_{0.5}$A [30]. Accordingly, this case is also marked with letter S. The instabilities can affect other 13 low *Le* flames.

Typical evolutions of the area-factor $\Sigma(t)$ and stretch factor $I(t)$ in the two unstable laminar flames are reported in Fig. 2. In both cases, $I(t) \approx \Sigma(t)$ during the linear stage of instability development, characterized by a rapid growth of both $I(t)$ and $\Sigma(t)$, but $I(t) > \Sigma(t)$ during a later quasi-steady stage, with this difference being much larger at $\Phi = 0.35$.

3.2. Turbulent flames

Fig. 3 reports time-dependencies of area factor $\Sigma(t)$ (black solid lines) and stretch factor $I(t)$ (red dashed lines) computed in 15 turbulent cases. Area factors obtained from equidiffusive flames are plotted in blue dotted lines. Results computed in case $\mathscr{L}\phi_{0.5}$A are not shown in Fig. 3, because they are very close to the results obtained from flame $\mathscr{D}_S\phi_{0.5}$A [30]. Time-averaged values of $\overline{U_T(t)}$, $\overline{\Sigma(t)}$, and $\overline{I(t)}$, calculated excluding initial evolution stages, are reported in Tables 2 and 3 at $\Phi = 0.5$ and 0.35, respectively. The following trends are worth noting.

First, with the exception of the weakly turbulent small-scale flame $\mathscr{D}_S\phi_{0.5}$B/$\mathscr{L}\phi_{0.5}$A(U), cf. black solid and blued dotted lines in Fig. 3o, the area-factor Σ in a low Lewis number flame is either statistically smaller than in its equidiffusive counterpart, see Fig. 3d-e and n, or $I(t)$ and $\Sigma(t)$ are comparable in both cases, see Fig. 3b, c, and m. As a low *Le* flame is characterized by a lower u'/S_L when compared to its equidiffusive counterpart, see Table 1, this difference does not explain the observed trends, because a smaller u'/S_L is associated with a smaller Σ, e.g., see Fig. 4a. The lower values of $\overline{\Sigma(t)}$, reported in low *Le* cases $\mathscr{D}_M\phi_{0.5}$B - $\mathscr{D}_M\phi_{0.5}$D and $\mathscr{D}_S\phi_{0.35}$B in Tables 2 and 3, may be attributed to lower ratios of L/δ_L^T in these flames when compared to their equidiffusive counterparts. Indeed, flame speed and surface area are known to be larger when this length-scale ratio is higher [10,13,44–47]. The values of $\overline{\Sigma(t)}$ obtained from groups I-IV and flame $\phi_{0.7}$ show this trend also, cf. L/δ_L^T in Table 1 and filled symbols in Fig. 4a.

Following suggestion by a Reviewer, an extra equidiffusive case $\mathscr{D}_L\phi_{0.43}$E1 was run by reducing Φ to counterbalance an increase in S_L with increasing *Le* from 0.39 to 1.0. However, the thickness δ_L^T is still larger in the equidiffusive flame. Comparison of results obtained from flames $\mathscr{D}_L\phi_{0.5}$E and $\mathscr{D}_L\phi_{0.43}$E1, see Fig. 3k and Table 2, shows almost

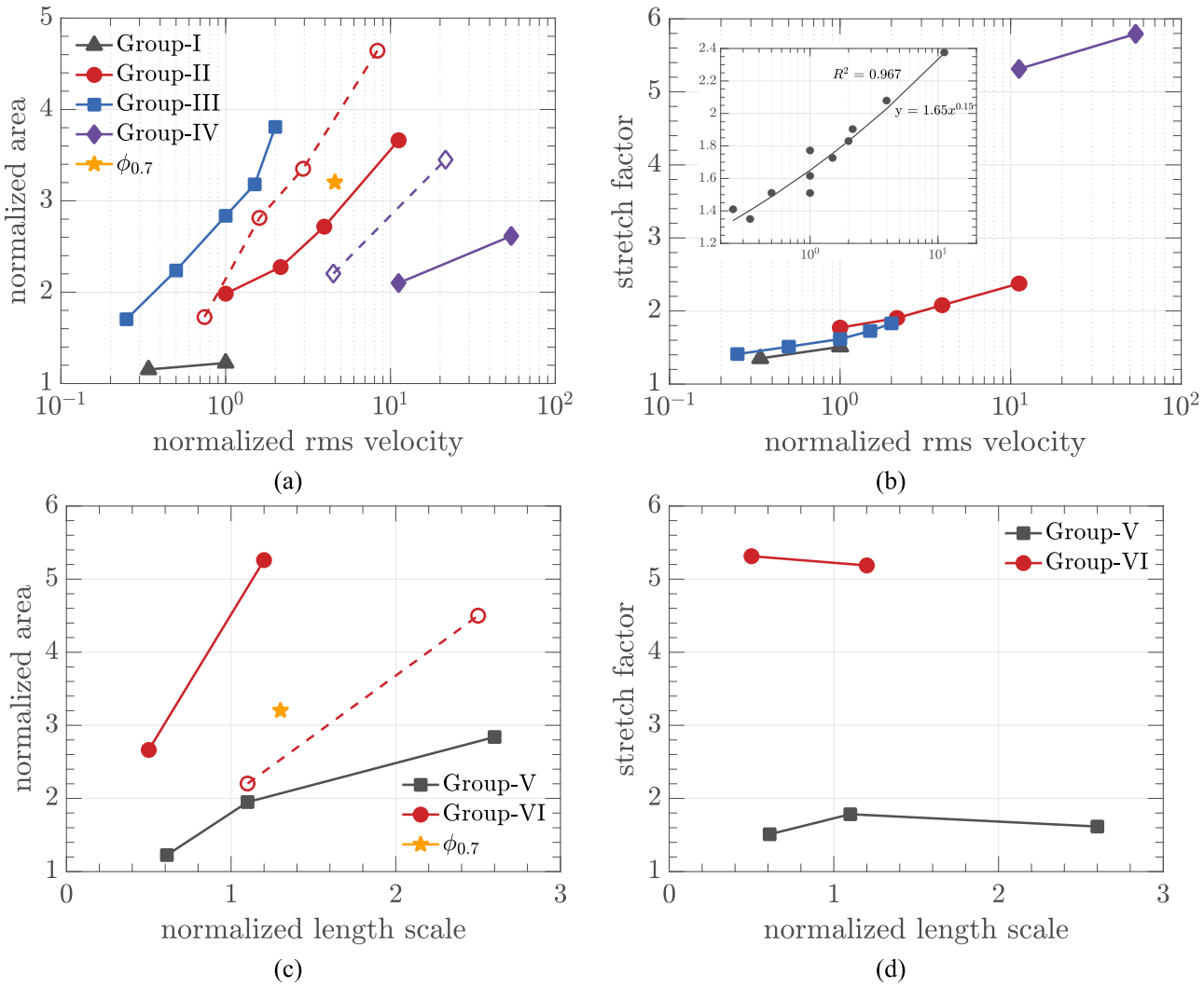

Fig. 4. Dependencies of time-averaged (a, c) area-factor $\overline{\Sigma(t)}$ and (b, d) stretch factor $\overline{I(t)}$ on normalized (a-b) rms velocity u'/S_L^0 and (c-d) length-scale L/δ_L^T, with the flame-group number being specified in legends. Open symbols and dashed lines show $\overline{\Sigma(t)}$ in equidiffusive flames.

equal $\overline{\Sigma(t)}$, thus, implying that the influence of a large difference in *Le* on the area-factor is counterbalanced by a moderate difference (about 25 %) in L/δ_L^T.

In any case, the present DNS data do not indicate a large increase in $\Sigma(t)$ with decreasing *Le*, whereas $I(t)$ is significantly larger than unity in low *Le* flames characterized by $\Phi = 0.35$ or 0.5 (in flame $\phi_{0.7}$, the mean $\overline{I(t)} = 1.45$). A stronger influence of *Le* on stretch factors when compared to flame surface areas was also reported in DNS studies of single-step chemistry flames [48] and complex-chemistry flames [19]. DNS data by Rieth et al. [20, Fig. 9c] also indicate a weak influence of *Le* on Σ.

Second, the time-averaged $\overline{\Sigma(t)}$ is significantly increased by u'/S_L^0 and L/δ_L^T both in low Lewis number flames, see filled symbols and solid lines in Fig. 4a and 4c, and in equidiffusive flames, see open symbols and dashed lines. To the contrary, the present DNS data do not reveal a notable dependence of the stretch factor I on L/δ_L^T, see Fig. 4d, but indicate a weak increase in I by u'/S_L^0, see Fig. 4b. Application of the power-law fitting $I \propto (u'/S_L^0)^q$ to the DNS data plotted in Fig. 4b yields $q = 0.10$ and $R^2 = 1.0$ (two points only), $q = 0.119 \pm 0.008$ and $R^2 = 0.995$, $q = 0.12 \pm 0.02$ and $R^2 = 0.988$, $q = 0.06$ and $R^2 = 1.0$ for flame groups I, II, III, and IV, respectively. For all these 13 flames fitted together, $q = 0.15 \pm 0.02$ and $R^2 = 0.967$, see insert in Fig. 4b. Recent DNS data by Howarth et al. [21, Fig. 21] show that the mean local consumption velocity $\overline{u}_c$ (evaluated by integrating the rate $\dot{\omega}_F(\mathbf{x}, t)$ along the local normal to flame surface, followed by ensemble-averaging), scales as $\overline{u}_c \propto (u'/S_L^0)^{3/4} (L/\delta_L^T)^{-1/4}$. These and the present results are consistent in two aspects: (i) the influence of differential diffusion on local burning rate is increased by u'/S_L^0 and (ii) this influence depends weaker on L/δ_L^T. However, the scaling exponents q obtained here are significantly less than the exponent $q = 3/4$ found by Howarth et al. [21]. This difference is not surprising, because the stretch factor I and the mean local consumption velocity $\overline{u}_c$ are different quantities and, hence, may exhibit quantitatively different scaling. For instance, I evaluated using Eq. (1) depends on the choice of an isoscalar surface associated with a flame front, whereas $\overline{u}_c$ does not. Moreover, substitution of I with $\overline{u}_c$ may make Eq. (1) wrong if the rate $\dot{\omega}_F(\mathbf{x}, t)$, which is integrated to find $\overline{u}_c$, correlates with $|\nabla c_F|$, which is linked with Σ.

Third, comparison of $I(t)$, see Fig. 3, or $\overline{I(t)}$, see Tables 2 and 3 or Fig. 4b and d, obtained from richer ($\Phi = 0.5$, groups I-III and V) and leaner ($\Phi = 0.35$, groups IV and VI) flames shows that the stretch factor is much higher in the leaner mixture. This trend is also observed in case $\phi_{0.7}$, where $\overline{I(t)} = 1.45$). Moreover, $I(t)$ obtained from leaner ($\Phi = 0.35$) turbulent flames $\mathscr{D}_S\phi_{0.35}$A/$\mathscr{L}\phi_{0.35}$A, $\mathscr{D}_S\phi_{0.35}$B, and $\mathscr{L}\phi_{0.35}$B is significantly higher than $I(t)$ in the counterpart unstable laminar flame, see Fig. 2b. At $\Phi = 0.5$, differences in the values of $I(t)$ obtained from

laminar and turbulent flames are smaller. Besides, in the latter case, Fig. 4b, d, and the scaling exponents q reported earlier, imply that dependence of the stretch factor I on u'/S_L^0 or L/δ_L^T could be neglected for modeling purposes to the leading order when compared to the significant influence of Φ on I.

Fourth, the present results do not show any notable difference between turbulent flames simulated in narrow domains where thermodiffusive instability cannot appear (cases $\mathscr{L}\phi_{0.5}$A(S) or $\mathscr{D}_S\phi_{0.35}$A/ $\mathscr{L}\phi_{0.35}$A and $\mathscr{D}_S\phi_{0.35}$B) and larger turbulent flame $\mathscr{D}_S\phi_{0.5}$B/ $\mathscr{L}\phi_{0.5}$A(U) or $\mathscr{L}\phi_{0.35}$B, respectively. Specifically, the stretch factors are comparable in flames $\mathscr{L}\phi_{0.5}$A(S) and $\mathscr{L}\phi_{0.5}$A(U) or $\mathscr{D}_S\phi_{0.35}$A/ $\mathscr{L}\phi_{0.35}$A, $\mathscr{D}_S\phi_{0.35}$B, and $\mathscr{L}\phi_{0.35}$B despite the instability can appear in the wider domain (flames $\mathscr{L}\phi_{0.5}$A(U) and $\mathscr{L}\phi_{0.35}$B) only. Besides, in the leanest case ($\Phi = 0.35$), the stretch factors are larger than 5, see Tables 2 and 3, i.e., are significantly larger than $I(t) \leq 3$ in the unstable laminar flame, see Fig. 2.

Finally, it is worth noting that weak dependence of $I(t)$ on L/δ_L^T, see black squares in Fig. 4d, where L/δ_L^T is varied by a factor of 4.3, is in line with a weak dependence of the stretch factor on the computational domain width, observed in a recent DNS of a laminar flame [49, Table 2]. These findings imply that the stretch factor is controlled by small-scale phenomena and, hence, is not very sensitive to confinement effects due to a finite computation domain width.

4. Conclusions

The present analysis of DNS data obtained earlier [11,23,25–30] shows that the flame surface area (i) is substantially increased by both turbulent rms velocity and length scale, (ii) is mainly controlled by turbulence, but (iii) is weaker affected by Lewis number. On the contrary, the stretch factor (i) is substantially larger than unity in low Lewis number flames, (ii) is significantly increased with decreasing equivalence ratio, and (iii) is weakly increased by rms velocity, but (iv) a notable influence of turbulence length scale on the stretch factor is not observed.

Novelty and significance statement

The novelty of this research consists in (i) systematically exploring effects of rms turbulent velocity, length scale, equivalence ratio, and Lewis number on flame surface area and stretch factor in lean H_2-air flames and (ii) showing that the area is primarily controlled by turbulence characteristics, whereas the stretch factor is primarily controlled by equivalence ratio and Le. These new results are significant for developing high-fidelity models of turbulent burning of lean H_2-air mixtures.

CRediT authorship contribution statement

H.C. Lee: Software, Validation, Investigation, Data curation, Writing – original draft, Visualization. **B. Wu:** Software, Data curation. **P. Dai:** Writing – review & editing, Supervision, Funding acquisition. **M. Wan:** Writing – review & editing, Supervision, Funding acquisition, Project administration, Conceptualization. **Andrei N. Lipatnikov:** Writing – original draft, Conceptualization, Supervision.

Declaration of competing interest

The authors declare that they have no known competing financial interests or personal relationships that could have appeared to influence the work reported in this paper.

Acknowledgments

AL gratefully acknowledges the financial support by Swedish Research Council (Grant No. 2023-04407) and Chalmers Area of Advance “Transport” (Grant No. 2021-0040). Other authors have been supported in part by NSFC (Grants No’s. 91752201, 51976088, and 92041001), the Shenzhen Science and Technology Program (Grants No’s. KQTD20180411143441009 and JCYJ20210324104802005), Department of Science and Technology of Guangdong Province (Grants No’s. 2019B21203001 and 2020B1212030001), National Science and Technology Major Project (Grants No’s. 539 J2019-II-0006-0026 and J2019-II-0013-0033), and the Center for Computational Science and Engineering of Southern University of Science and Technology.

References

[1] N. Peters, Turbulent Combustion, Cambridge University Press, Cambridge, UK, 2000.
[2] T. Poinsot, D. Veynante, Theoretical and Numerical Combustion, 2nd ed., Edwards, Philadelphia, PA, 2005.
[3] R.W. Bilger, S.B. Pope, K.N.C. Bray, J.F. Driscoll, Paradigms in turbulent combustion research, Proc. Combust. Inst. 30 (2005) 21–42.
[4] J.F. Driscoll, Turbulent premixed combustion: flamelet structure and its effect on turbulent burning velocities, Prog. Energy Combust. Sci. 34 (2008) 91–134.
[5] G. Damköhler, Der einfuss der turbulenz auf die flammengeschwindigkeit in gasgemischen, Z. Electrochem. 46 (1940) 601–652.
[6] K.N.C. Bray, R.S. Cant, Some applications of Kolmogorov’s turbulence research in the field of combustion, Proc. R. Soc. Lond. A434 (1991) 217–240.
[7] D. Bradley, How fast can we burn? Proc. Combust. Inst. 24 (1992) 247–262.
[8] G.V. Nivarti, R.S. Cant, Direct numerical simulation of the bending effect in turbulent premixed flames, Proc. Combust. Inst. 36 (2017) 1903–1910.
[9] A.N. Lipatnikov, V.A. Sabelnikov, An extended flamelet-based presumed probability density function for predicting mean concentrations of various species in premixed turbulent flames, Int. J. Hydrog. Energy 45 (2020) 31162–31178.
[10] W. Song, F.E. Hernández Pérez, E.-Al. Tingas, H.G. Im, Statistics of local and global flame speed and structure for highly turbulent H_2/air premixed flames, Combust. Flame 232 (2021) 111523.
[11] H.C. Lee, P. Dai, M. Wan, A.N. Lipatnikov, Displacement speed, flame surface density, and burning rate in highly turbulent premixed flames characterized by low Lewis numbers, J. Fluid Mech. 961 (2023) A21.
[12] S. Chaudhuri, B. Savard, Turbulent flame speed based on the mass flow rate: theory and DNS, Combust. Flame 252 (2023) 112735.
[13] A.N. Lipatnikov, J. Chomiak, Turbulent flame speed and thickness: phenomenology, evaluation, and application in multi-dimensional simulations, Prog. Energy Combust. Sci. 28 (2002) 1–73.
[14] V.R. Kuznetsov, V.A. Sabel’nikov, Turbulence and Combustion, Hemisphere Publ. Corp., New York, 1990.
[15] A. Lipatnikov, Fundamentals of Premixed Turbulent Combustion, CRC Press, Boca Raton, FL, 2012.
[16] S. Hochgreb, How fast can we burn, 2.0? Proc. Combust. Inst. 29 (2023) 2077–2105.
[17] D. Bradley, A.K.C. Lau, M. Lawes, Flame stretch rate as a determinant of turbulent burning velocity, Philos. Trans. R. Soc. Lond.. A338 (1992) 359–387.
[18] A.N. Lipatnikov, J. Chomiak, Molecular transport effects on turbulent flame propagation and structure, Prog. Energy Combust. Sci. 31 (2005) 1–73.
[19] L. Berger, A. Attili, H. Pitsch, Synergistic interactions of thermodiffusive instabilities and turbulence in lean hydrogen flames, Combust. Flame 244 (2022) 112254.
[20] M. Rieth, A. Gruber, J.H. Chen, The effect of pressure on lean premixed hydrogen-air flames, Combust. Flame 250 (2023) 112514.
[21] T.L. Howarth, E.F. Hunt, A.J. Aspden, Thermo-diffusively-unstable lean premixed hydrogen flames: phenomenology, empirical modelling, and thermal leading points, Combust. Flame 253 (2023) 112811.
[22] V. Coulon, J. Gaucherand, V. Xing, D. Laera, C. Lapeyre, T. Poinsot, Direct numerical simulations of methane, ammonia-hydrogen and hydrogen turbulent premixed flames, Combust. Flame 256 (2023) 112933.
[23] H.C. Lee, P. Dai, M. Wan, A.N. Lipatnikov, A numerical support of leading point concept, Int. J. Hydrog. Energy 47 (2022) 23444–23461.
[24] M. Rieth, A. Gruber, F.A. Williams, J.H. Chen, Enhanced burning rates in hydrogen-enriched turbulent premixed flames by diffusion of molecular and atomic hydrogen, Combust. Flame 239 (2022) 111740.
[25] H.C. Lee, P. Dai, M. Wan, A.N. Lipatnikov, Influence of molecular transport on burning rate and conditioned species concentrations in highly turbulent premixed flames, J. Fluid Mech. 928 (2021) A5.
[26] H.C. Lee, P. Dai, M. Wan, A.N. Lipatnikov, A DNS study of extreme and leading points in lean hydrogen-air turbulent flames - part I: local thermochemical structure and reaction rates, Combust. Flame 235 (2022) 111716.
[27] H.C. Lee, P. Dai, M. Wan, A.N. Lipatnikov, A DNS study of extreme and leading points in lean hydrogen-air turbulent flames - part II: local velocity field and flame topology, Combust. Flame 235 (2022) 111712.
[28] H.C. Lee, P. Dai, M. Wan, A.N. Lipatnikov, Lewis number and preferential diffusion effects in lean hydrogen-air highly turbulent flames, Phys. Fluids 34 (2022) 035131.
[29] H.C. Lee, A. Abdelsamie, P. Dai, M. Wan, A.N. Lipatnikov, Influence of equivalence ratio on turbulent burning velocity and extreme fuel consumption rate in lean hydrogen-air turbulent flames, Fuel 327 (2022) 124969.

[30] H.C. Lee, B. Wu, P. Dai, M. Wan, A.N. Lipatnikov, Turbulent burning velocity and thermodiffusive instability of premixed flames, Phys. Rev. E 108 (2023) 035101.
[31] A. Abdelsamie, G. Fru, T. Oster, F. Dietzsch, G. Janiga, D. Thévenin, Towards direct numerical simulations of low-Mach number turbulent reacting and two-phase flows using immersed boundaries, Comput. Fluids 131 (2016) 123–141.
[32] A. Kéromnès, W.K. Metcalfe, K.A. Heufer, N. Donohoe, A.K. Das, C.-J. Sung, J. Herzler, C. Naumann, P. Griebel, O. Mathieu, M.C. Krejci, E.L. Petersen, W. J. Pitz, H.J. Curran, An experimental and detailed chemical kinetic modeling study of hydrogen and syngas mixture oxidation at elevated pressures, Combust. Flame 160 (2013) 995–1011.
[33] D. Goodwin, N. Malaya, H. Moffat, R. Speth, Cantera: an Object-Oriented Software Toolkit For Chemical Kinetics, Thermodynamics, and Transport Processes, Caltech, Pasadena, CA, 2009.
[34] T.S. Lundgren, Linearly forced isotropic turbulence. Center for Turbulence Research Annual Research Brief, 2003, pp. 461–473. https://ntrs.nasa.gov/api/citations/20040031711/downloads/20040031711.pdf.
[35] C. Rosales, C. Meneveau, Linear forcing in numerical simulations of isotropic turbulence: physical space implementations and convergence properties, Phys. Fluids 17 (2005) 095106.
[36] P.L. Carroll, G. Blanquart, The effect of velocity field forcing techniques on the Karman-Howarth equation, J. Turbul. 15 (2014) 429–448.
[37] B. Bobbitt, S. Lapointe, G. Blanquart, Vorticity transformation in high Karlovitz number premixed flames, Phys. Fluids 28 (2016) 015101.
[38] B. Bobbitt, G. Blanquart, Vorticity isotropy in high Karlovitz number premixed flames, Phys. Fluids 28 (2016) 105101.
[39] J. Chomiak, A.N. Lipatnikov, A simple criterion of importance of laminar flame instabilities in premixed turbulent combustion of mixtures characterized by low Lewis numbers, Phys. Rev. E 107 (2023) 015102.
[40] L.D. Landau, E.M. Lifshitz, Fluid Mechanics, Pergamon Press, Oxford, 1987.
[41] C.E. Frouzakis, N. Fogla, A.G. Tomboulides, C. Altantzis, M. Matalon, Numerical study of unstable hydrogen/air flames: shape and propagation speed, Proc. Combust. Inst. 35 (2015) 1087–1095.
[42] L. Berger, A. Attili, H. Pitsch, Intrinsic instabilities in premixed hydrogen flames: parametric variation of pressure, equivalence ratio, and temperature. Part 1 - Dispersion relations in the linear regime, Combust. Flame 240 (2022) 111935.
[43] A.N. Lipatnikov, H.C. Lee, P. Dai, M. Wan, V.A. Sabelnikov, Transition from turbulence-dominated to instability-dominated combustion regime in lean hydrogen-air flames, Combust. Flame 259 (2024) 113170.
[44] R. Yu, A.N. Lipatnikov, DNS study of dependence of bulk consumption velocity in a constant-density reacting flow on turbulence and mixture characteristics, Phys. Fluids 29 (2017) 065116.
[45] J. Kim, A. Satija, R.P. Lucht, J.P. Gore, Effects of turbulent flow regime on perforated plate stabilized piloted lean premixed flames, Combust. Flame 211 (2020) 158–172.
[46] A.R. Varma, U. Ahmed, M. Klein, N. Chakraborty, Effects of turbulent length scale on the bending effect of turbulent burning velocity in premixed turbulent combustion, Combust. Flame 233 (2021) 111569.
[47] A.N. Lipatnikov, V.A. Sabelnikov, F.E. Hernández-Pérez, W. Song, H.G. Im, A priori DNS study of applicability of flamelet concept to predicting mean concentrations of species in turbulent premixed flames at various Karlovitz numbers, Combust. Flame 222 (2020) 370–382.
[48] N. Chakraborty, A.N. Lipatnikov, Effects of Lewis number on conditional fluid velocity statistics in low Damköhler number turbulent premixed combustion: a Direct Numerical Simulation analysis, Phys. Fluids 25 (2013) 045101.
[49] X. Wen, L. Berger, L. Cai, A. Parente, H. Pitsch, Thermodiffusively unstable laminar hydrogen flame in a sufficiently large 3D computational domain – Part I: characteristic patterns, Combust. Flame 263 (2024) 113278.